

Article

Green Synthesis of *Cocos nucifera*-Based Nanomaterials and Mechanistic Basis of Their Antimicrobial Action

Zuriatou Yajeh Tanka ¹, Naphtali Odogu Ankoro ², Vincent Ngouana ³, Franklin Loïc Tchinda Taghu ¹, Abongta Lum Mforbesi ¹, Branly-Natalien Nguena-Dongue ¹, Julius Nsami Ndi ², Boniface Pone Kamdem ^{1,*}, Paul Keilah Lunga ^{1,*} and Fabrice Fekam Boyom ¹

- ¹ Antimicrobial and Biocontrol Agents Unit (AmBcAU), Laboratory for Phytobiochemistry and Medicinal Plants Studies, Department of Biochemistry, Faculty of Science, University of Yaounde I, Yaounde P.O. Box 812, Cameroon; nguenadonguebranlynatalien@gmail.com (B.-N.N.-D.); fabrice.boyom@fulbrightmail.org (F.F.B.)
- ² Applied Physical and Analytical Chemistry Laboratory, Department of Inorganic Chemistry, Faculty of Science, University of Yaounde I, Yaounde P.O. Box 812, Cameroon; ndinsami2002@gmail.com (J.N.N.)
- ³ Department of Pharmacy, Faculty of Medicine and Pharmaceutical Sciences, University of Dschang, Dschang P.O. Box 96, Cameroon
- * Correspondence: ponekamdemboniface@gmail.com (B.P.K.); lungapaul@yahoo.ca (P.K.L.); Tel.: +(237)-680-98-76-69 (B.P.K.); +(237)-672-46-01-30 (P.K.L.)

Abstract: Caused by pathogenic microorganisms, infectious diseases are known to cause high mortality rates, severe burdens of disability, and serious worldwide aftermaths. Drug-resistant pathogens have reduced the efficacy of available therapies against these diseases, thus accentuating the need to search for effective antimicrobials. Medicinal plants have served as starting material for the preparation of a number of antimicrobial agents. To this end, the present study highlights the green synthesis of *Cocos nucifera*-based nanomaterials and evaluation of the mechanistic basis of their antimicrobial action. Accordingly, *Cocos nucifera* extract was used for the reduction of silver nitrate solution to afford silver nanoparticles. These entities were further incorporated onto sulfuric-acid-based activated carbons to generate the nanocomposites. The antimicrobial activity of the as-prepared nanomaterials was evaluated using the broth microdilution method, while the antioxidant activity was assessed through standard methods. The cytotoxicity of potent nanomaterials was assessed on Vero cells by the spectrophotometric method. As a result, nanoparticles were successfully synthesized, as evidenced by the ultraviolet–visible spectroscopy analysis that revealed an intense absorption spectrum at 433 nm. Fourier Transform Infrared Spectroscopy presented the functional group moieties involved as a capping and reducing agent in the synthesis of the nanomaterials. The incubation of nanomaterials with selected bacterial and fungal strains has led to significant inhibitory effects of these pathogens with minimum inhibitory concentrations ranging from 7.813 to 250 µg/mL. In antioxidant assays, the nanocomposites presented scavenging activities comparable to those of ascorbic acid. Cytotoxicity experiment revealed no toxic effects on Vero cells (range of selectivity indices: from >4 to >128). These results provide evidence of the implication of *Cocos nucifera*-based nanomaterials in targeting bacterial or fungal systems that mediate free-radical damage or by inhibiting the oxidative damage caused by selected bacteria and fungi, the most susceptible being *Escherichia coli* and *Candida albicans*, respectively.

Keywords: *Cocos nucifera*; green synthesis; nanomaterials; activated carbon; antimicrobial activity; cytotoxicity; oxidative stress



Citation: Yajeh Tanka, Z.; Ankoro, N.O.; Ngouana, V.; Tchinda Taghu, F.L.; Mforbesi, A.L.; Nguena-Dongue, B.-N.; Nsami Ndi, J.; Pone Kamdem, B.; Keilah Lunga, P.; Fekam Boyom, F. Green Synthesis of *Cocos nucifera*-Based Nanomaterials and Mechanistic Basis of Their Antimicrobial Action. *BioMed* **2024**, *4*, 59–77. <https://doi.org/10.3390/biomed4010005>

Academic Editor: Wolfgang Graier

Received: 31 January 2024

Revised: 24 February 2024

Accepted: 28 February 2024

Published: 6 March 2024



Copyright: © 2024 by the authors. Licensee MDPI, Basel, Switzerland. This article is an open access article distributed under the terms and conditions of the Creative Commons Attribution (CC BY) license (<https://creativecommons.org/licenses/by/4.0/>).

1. Introduction

Infectious diseases are the most frequent diseases, representing an important cause of morbidity and mortality among the general population, particularly in developing countries [1,2]. Infectious diseases are predominant in African and Asian countries due to the

most prevalent vulnerable population, poor hygienic conditions, inadequate funding, poor microbiology services, limited technical experts, and scarce epidemiological data to better inform preventive and treatment strategies [3]. Bongomin et al. [4] reported that patients with compromised immune function are especially prone to fungal pathogens, which account for at least 13 million infections and 1.5 million deaths in the world annually [4]. Annually, over 150 million severe cases of fungal infections occur worldwide, resulting in approximately 1.7 million deaths per year [5]. Data generated by the Global Action Funds for Fungal Infections (GAFFI) suggest an estimated 47.6 million Africans suffer from fungal diseases [6]. In Cameroon, it is estimated that more than a million people are affected each year by serious fungal infection, among which 8.1% of cases of recurrent vulvovaginal candidiasis are reported in women aged 15 to 50 years [7]. On the other hand, deaths caused by bacterial infections accounted for more than one in eight global deaths in 2019, with five pathogens (*Staphylococcus aureus*, *Escherichia coli*, *Streptococcus pneumoniae*, *Klebsiella pneumoniae*, and *Pseudomonas aeruginosa*) accounting for more than half of those deaths [8]. In 2019, bacterial infections caused most deaths in sub-Saharan Africa, with an estimated 230 deaths per 100,000 people [9]. Recently, AMvomo et al. [10] reported that out of 156 samples collected from a Jordan Hospital (Yaounde-Cameroon), 86 were cultured positive, and 100 bacteria, including mostly *Enterobacter cloacae* (17%), *Klebsiella pneumoniae* (17%), *Staphylococcus aureus* (16%), and *Escherichia coli* (11%), were isolated [10].

Nowadays, various antimicrobial agents including antibiotics have been widely employed in treating diseases caused by these infectious pathogens. These include antifungal drugs, such as amphotericin B, fluconazole, itraconazole, voriconazole, and posaconazole [11], as well as antibacterial therapies like the fluoroquinolones (ciprofloxacin, moxifloxacin, norfloxacin, etc.), penicillins (amoxicillin, dicloxacillin, etc.), aminoglycosides (amikacin, gentamicin, tobramycin), and cephalosporins (ceftriaxone, cefepime, ceftazidime), and others. Moreover, combination therapies would be recommended for multi-drug-resistant bacterial (ceftriaxone–vancomycin [12]; ceftolozane–tazobactam, meropenem–vaborbactam, aztreonam–avibactam, and imipenem–cilastatin–relebactam [13], among others) and fungal (AmB–posaconazole [14]; flucytosine–amphotericin B, flucytosine–azoles, and AmB–rifampin, and others [15]) infections. However, the misuse and/or excessive use of these antimicrobials has developed drug resistance, resulting in low treatment efficacy. The growing resistance of microbes to antibacterial and antifungal treatments, as well as their toxic effects, suggested imperatively to search for alternative remedies against these maladies [16]. Even though the antimicrobial drugs that possess antioxidant properties might help in the fight against microbial drug resistance, the side effects of these antioxidants (ethoxyquin and propyl gallate are carcinogenic, neurotoxic, hepatotoxic, etc.) are not negligible.

Medicinal plants have been used for several decades to cure a variety of diseases, including bacterial and fungal diseases [17]. In addition, contemporary medicines derive basically from herbs with reference to traditional knowledge, practices, and beliefs. According to the World Health Organization (WHO), more than 80% of the world's population relies on traditional medicine for their basic health care [18]. One such plant is *Cocos nucifera*, which is used for the traditional treatment of diarrhea and stomach aches, and as a topic ointment for dermatitis, abscesses, injuries, etc. [19]. On the other hand, modern chemistry and pharmacological studies have demonstrated the implication of active principles from diverse sources (especially, from plants) in the discovery of antimicrobial drugs [17,20]. For instance, previous reports have demonstrated the anti-inflammatory, antiviral, anthelmintic, antileishmanial, antimalarial, and hepatoprotective activities of *Cocos nucifera* [19].

Materials in the nanoscale range have been employed to deliver therapeutic agents to specific targeted sites in a well-ordered method [21]. These nanoparticles have created huge interest in a wide range of applications owing to their controllable size and shape, along with excellent reactivity and unique physical, chemical, and biological properties [16]. Because of their nano size and large surface-to-volume ratio, silver nanoparticles have been described to exhibit antimicrobial action against a wide range of bacterial and fungal

strains [22–24]. Although metal-based nanoparticles have been reported to exhibit antimicrobial activity against bacterial and fungal diseases [25–27], biocapping with plant extracts is an effective approach for the fabrication of nanoparticles with minimum toxicity [28,29]. More recently, new approaches have been developed to enhance the antimicrobial activity of nanoscale materials by tagging nanoparticles on the surface of activated carbon to acquire nanocomposites [30]. Moreover, it is well known that nanocomposites exhibit more efficient antibacterial activity than their nanoparticle counterparts [30]. Indeed, activated carbon (AC) is a porous material exhibiting amphoteric characteristics and is usually used for the adsorption of organic and inorganic compounds. Additionally, activated carbons have the ability to adsorb bacteria, fungi, toxins, and other chemicals [31].

Furthermore, there is evidence that antioxidant compounds, such as phenolics, flavonoids, alkaloids, fatty acids, tannins, terpenoids, and steroids are accountable for the antimicrobial activity of plant extracts [32,33]. Indeed, a variety of antioxidant metabolites, including flavonoids [19,34], terpenoids [19,35], and phenolic compounds [36], were reported in *Cocos nucifera* L. These compounds are well known to exert antimicrobial activity via a number of mechanisms, including bacterial or fungal membrane damage, inhibition of virulence factors (enzymes and toxins) and nucleic acid synthesis, leakage of cellular components, and inhibition and eradication of bacterial biofilm formation, among others [37–40].

Based on the foregoing, there is evidence that biologically synthesized nanomaterials (nanoparticles and nanocomposites) can afford potentially active antimicrobial compounds that might serve as a baseline for the discovery of effective antimicrobial agents. Thus, the present study aims to synthesize *Cocos nucifera*-based nanomaterials and study the mechanistic basis of their antimicrobial action. Antioxidant and cytotoxicity studies of the nanomaterials were also evaluated.

2. Material and Methods

2.1. Material

Shells of *Cocos nucifera* (coconut shells) were obtained from coconut vendors in the local Melen market, Mfoundi Division, Centre Region of Cameroon. These shells were brought to the Physical and Theoretical Chemistry Laboratory of the University of Yaoundé 1 and used for the preparation of activated carbon and nanomaterials. The coconut shells were washed to remove dirt and other contaminants and then dried to remove water and moisture. Next, the shells were ground mechanically using a Retsch Pulverisette grinder (RETSCH, Haan, Germany) (2.2 kW and 1500 rpm), sieved to sizes varying between 0–1.25 mm and 1.25–2.5 mm, and then stored at room temperature for further use.

2.2. Preparation of the Activated Carbon

The activated carbon was prepared according to a previously reported method by Naphtali Odogu et al. [41]. Ten grams (10.0 g) of the ground coconut shells were impregnated with H₂SO₄ (98%) solution of impregnation ratio 0.5. The mixture was kept for 1 h at room temperature so that reagents were fully absorbed into the shells' network. The impregnated sample was dried at 110 °C for 24 h in an oven. The dried impregnated samples were cooled in a desiccator for 1 h and carbonized using a Carbolite Furnace at a temperature of 432 °C for 40 min. The activated carbon (AC) obtained was washed with distilled water.

2.3. Synthesis and Characterization of Silver Nanoparticles

Silver nanoparticles (AgNP) were prepared using aqueous coconut shell extract as the reducing agent and silver nitrate (AgNO₃) as the precursor reagent, as per a standard protocol reported by Das et al. [42] with minor modifications (by using 5, 10, and 20 mM of AgNO₃ in lieu of 1 mM of AgNO₃). Briefly, 10.0 g of the powder coconut shells was mixed with 100 mL of distilled water, then stirred using a magnetic stirrer for 30 min, and filtered. Next, about 100 mL AgNO₃ (5, 10 and 20 mM) was taken in 3 separate sets of the conical flask (250 mL) and then the addition of coconut shell solution (10 mL) was

effected with constant stirring in a magnetic stirrer. The silver nanoparticle thus synthesised was characterised using ultraviolet–visible (UV–Vis) spectroscopy and Fourier Transform Infrared Spectroscopy (FTIR).

2.4. Preparation of Silver Nanocomposite

The nanoparticles (AgNPs) were loaded on the activated carbon by simple agitation. In brief, 5.0 g of activated carbon was added to the as-prepared AgNPs' solution. Then, the mixture was stirred continuously for 1 h at 150 rpm using a Horseshoe IKA agitator. The nanocomposite (AgNC) was further obtained by drying the AgNP-loaded activated carbon powder in an oven (Bluepard Instruments Co. Ltd., Shanghai, China) at 110 °C.

2.5. Antimicrobial Assay

2.5.1. Microbial Species and Culture Media

Eight bacteria species were used in this study. One strain (*Klebsiella pneumoniae* NR 41817, *Pseudomonas aeruginosa* NR 48982, *Shigella flexneri* NR 518, and *Shigella sonnei* NR 519) were obtained from the Biodefense and Emerging Infections Research Resources Repository (BEI Resources, Rockville, MD 20852, USA), whereas *Escherichia coli* (ATCC 25922) and *Staphylococcus aureus* (ATCC 43,310 and ATCC 33591) were obtained commercially from the American Type Culture Collection (ATCC, Manassas, VA, USA). Moreover, *Salmonella enteritidis* (CPC) was obtained from the Centre Pasteur of Cameroon. In addition, five fungal species, including *Candida albicans* (CA NR-29456), *Candida glabrata* (CG 100), *Candida parapsilosis* (CP O31S) (obtained from BEI Resources), *Candida albicans* (CA ATCC-14516), and *Candida krusei* (CK ATCC-1415) (obtained from ATCC), were also used in this study.

2.5.2. Determination of Minimum Inhibitory Concentrations

The minimum inhibitory concentrations (MICs) of the as-prepared nanomaterials were determined by the broth microdilution method (in triplicate) on 96-well microplates according to the M07A3 and M07A9 protocols described by the Clinical Laboratory Standards Institute [43]. Briefly, 196 µL of Mueller Hinton Broth and Sabouraud Dextrose Broth (MHB/SDB) was separately introduced into the wells of the first line of microplate, followed by the addition of 4 µL of different concentrations of nanomaterials (initially prepared at 100 mg/mL in distilled water). Next, two-fold serial dilutions were performed in the wells, and 100 µL of the bacterial (1.5×10^8 CFU/mL) or fungal suspension (2.5×10^3 CFU/mL) was added into each well. The final concentrations ranged from 1000 to 15.625 µg/mL for the nanomaterials and 2 to 0.0156 µg/mL for the positive controls (ciprofloxacin and fluconazole for antibacterial and antifungal tests, respectively). Then, the plates were incubated at 37 °C for 24 h and 4 h for bacterial and fungal strains, respectively, followed by an addition of 20 µL of 0.015 mg/mL resazurin solution (0.15 mg/mL in phosphate buffer saline, PBS) (Sigma-Aldrich, Darmstadt, Germany) and 30 min incubation at 37 °C. The minimum inhibitory concentrations (MICs) were determined as the lowest concentrations of nanomaterials or standard drugs at which no visible color change (from blue to pink) was observed. Wells containing MHB and bacteria, or SDB and fungi, constituted the negative control for antibacterial and antifungal tests, respectively, while the sterility controls contained only MHB and SDB.

2.6. Time–Kill Kinetics Test

The time–kill kinetic study of the most active nanoparticles and nanocomposites was performed on *E. coli* according to the method described by Nguimatsia et al. [18]. Herein, the active nanomaterials were prepared at various concentrations (MIC, 2MIC and 4MIC), by two-fold serial dilutions in a 96-well microplate. One hundred microliters (100 µL) of *E. coli* suspension (1.5×10^6 CFU/mL) was added to the preparations, and the plate was subsequently incubated at 37 °C at different time intervals (0, 1, 2, 4, 6, 8, 12, and 24 h). Following each incubation period, optical densities (OD) were read using a microtiter plate

reader (TECAN Infinite M200, Männedorf, Switzerland). The values obtained (optical densities) were used to draw a graph, i.e., OD versus incubation time at 630 nm.

2.7. Cytotoxicity Assays

As previously reported by Bowling et al. [44], the cytotoxicity of the most active nanomaterials was assessed by the resazurin colorimetric method, using the human mammalian cells Vero (ATCC CRL 1586), which were generously obtained from the Centre Pasteur of Cameroon (CPC). The Vero cells were cultured in complete medium containing 13.5 g/L DMEM (Gibco, Waltham, MA USA), 10% fetal bovine serum (Gibco, Waltham, MA USA), 0.21% bicarbonate (Sigma-Aldrich, New Delhi, India), and 10 mL (1%) of penicillin/streptomycin antibiotics. Noteworthy, the assay was performed in triplicate on 96-well cell-culture-treated microplates. In brief, a 100 μ L cell suspension, which was titrated at 5×10^3 cells/well using a Neubauer chamber, was introduced into the wells of a microplate 4 h prior to exposure with the most active nanomaterials to allow adhesion and cell confluence. Subsequently, the nanomaterials (100 μ L), which were prepared at different concentrations, were introduced into the wells containing the adherent cells and further incubated for 48 h at 37 °C in a humidified atmosphere with 5 % CO₂. The positive control and negative control wells contained podophyllotoxin at 10 μ M and cells without nanomaterials, respectively. Afterwards, 10 μ L of a solution of resazurin (0.15 mg/mL in PBS) was added into each well and then incubated for an additional 4 h. Fluorescence of the obtained preparation was measured at excitation and emission wavelengths of 530 and 570 nm, respectively, using a microtiter plate reader (TECAN Infinite M200, Männedorf, Switzerland). From the resulting values of fluorescence intensities, the percentage of cell viability was calculated with Microsoft Excel software using the following formula:

$$\% \text{ cell viability} = \frac{A_t - A_b}{A_c - A_b} \times 100$$

where A_t = absorbance of test sample, A_b = absorbance of the positive control podophyllotoxin, and A_c = absorbance of negative control (cells).

A dose–response curve (percentage of cell viability versus concentration of the nanomaterials) was plotted using graph pad prism software, to determine the median cytotoxic concentrations (CC₅₀s) of the test samples. The test was performed in triplicate on 96-well cell-culture-treated microplates.

2.8. In Vitro Antioxidant Activity

The antioxidant activity of the most active nanomaterials was evaluated using the 2,2-diphenyl-1-picrylhydrazyl (DPPH) and 2,2'-azino-bis(3-ethylbenzothiazoline-6-sulfonic acid (ABTS) radical scavenging assays.

2.8.1. DPPH Radical Scavenging Assay

A previously described protocol by Bassene [45] was used to evaluate the potential of the most active nanomaterials as scavengers of the free radicals of DPPH. Briefly, different concentrations (2000, 1000, 500, 250, 125, 62.5, 31.25, and 15.625 μ g/mL) of the nanomaterials were prepared in a 96-well microplate. Next, twenty-five microliters (25 μ L) of each solution was introduced into a fresh microplate, followed by an addition of 75 μ L of 0.02% DPPH to achieve final concentrations of 500, 250, 125, 62.5, 31.25, 15.625, 7.813, and 3.906 μ g/mL. The reaction mixtures were kept in the dark at room temperature for 30 min, and then the absorbance was measured at 517 nm against the blank (DPPH in methanol) using a microtiter plate reader (TECAN Infinite M200, Männedorf, Switzerland). L-ascorbic acid (concentration range: 25–0.195 μ g/mL) was used as the positive control. The assay was performed in triplicate, and the percentages (%) of radical scavenging activities of the test samples were calculated using the following formula:

$$\% \text{ RSA} = \frac{A_o - A_s}{A_o} \times 100$$

where RSA: radical scavenging activity; Ao: absorbance of the blank; and As: absorbance of test sample.

The radical scavenging activity 50 (RSA₅₀), effective concentration 50 (EC₅₀), and antiradical power (ARP) were further deduced from the % RSA.

2.8.2. ABTS Radical Scavenging Assay

A previously described method by Khan et al. [46] was used to assess the scavenging potential of the active antibacterial nanomaterials vis-à-vis free radicals of ABTS. In short, different concentrations (2000, 1000, 500, 250, 125, 62.5, 31.25, and 15.625 µg/mL) of the active nanomaterials were prepared in a 96-well microplate. Then, 25 µL of each solution was introduced into another microplate, followed by an addition of and 75 µL of 0.02% ABTS to obtain final concentrations of 500, 250, 125, 62.5, 31.25, 15.625, 7.813, and 3.906 µg/mL. After 30 min incubation at room temperature in the dark, the absorbance was read at 734 nm against the blank (ABTS in methanol) using a microtiter plate reader (TECAN Infinite M200, Männedorf, Switzerland). L-ascorbic acid (concentration range: 25–0.195 µg/mL) was used as the positive control. The assay was performed in triplicate, and the percentages (%) of radical scavenging activities of test samples were calculated using the following formula:

$$\% \text{ RSA} = \frac{A_o - A_s}{A_o} \times 100$$

where RSA: radical scavenging activity; Ao: absorbance of the blank; As: absorbance of test sample.

2.9. Statistical Analysis

Wherever appropriate, the data were subjected to one-way analysis of variance (ANOVA) and results were presented as the mean ± SD of the replicated values. Significant differences for multiple comparisons were determined by Dunnett test at $p \leq 0.001$ MIC, and CC₅₀ values were obtained as already discussed from the graphs plotted using Graph Pad prism version 8.0 (version 2013, Washington, DC, USA). Graphical evaluation of the data was conducted using Microsoft Excel 2016.

3. Results and Discussion

3.1. Results

3.1.1. UV-Visible Spectral Analysis

A biological synthesis of silver nanoparticles was successfully achieved using an aqueous extract of *Cocos nucifera* shells with silver nitrate (AgNO₃) solution at various concentrations (5, 10, and 20 mM) (Figure 1). The formation of the nanoparticle was evidenced by a gradual color change (from colorless to dark brown) that was observed. The fabrication of the AgNPs was further confirmed by UV-vis visible spectroscopy in the wavelength range of 350–900 nm (Figure 2). The absorption spectrum of the prepared silver nanoparticles showed surface Plasmon resonance and exhibited a λ_{max} at 433 nm, confirming the synthesis of the nanoparticles.

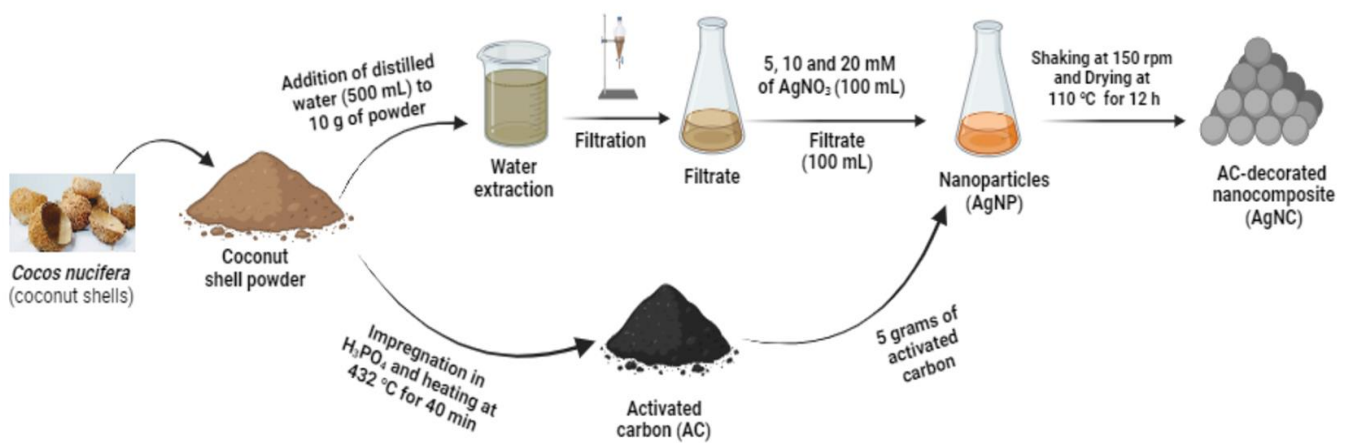


Figure 1. Graphical representation of the preparation of extract, silver nanoparticles, and nanocomposites from *Cocos nucifera* shells.

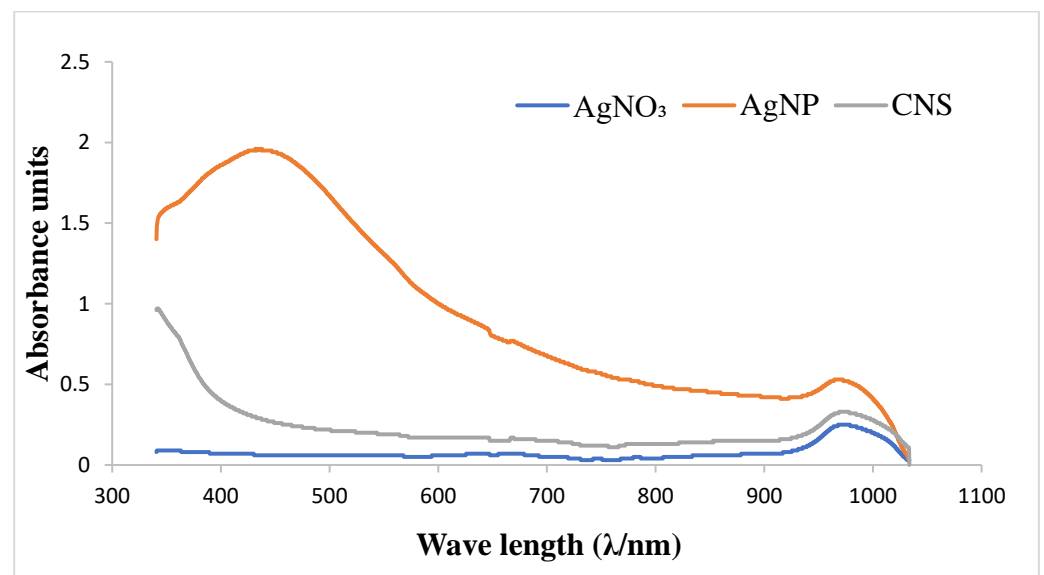


Figure 2. UV-Vis spectra of *Cocos nucifera* extract (CNS) compared with that of nanoparticles (AgNP) and chemical reagent (AgNO_3). AgNO_3 : silver nitrate; AgNP: silver nanoparticles; CNS: *Cocos nucifera* extract.

3.1.2. FTIR Analysis of Synthesized Nanomaterials

The FT-IR spectra of *Cocos nucifera* extract and nanoparticles (A), as well as activated carbon and nanocomposites (B), are presented in Figure 3. The *Cocos nucifera* extract displayed four adsorption peaks at 3297.338, 2923.413, 1643.004, and 1237.918 cm^{-1} . The band at 3297.338 cm^{-1} is due to the absorption of water molecules as result of an O-H stretching mode of hydroxyl groups and adsorbed water. A vibration band at 2923.413 cm^{-1} is attributed to the presence of methylene groups (C-H). Also, the 1643.004 cm^{-1} band is attributed to a carbonyl (C=O) of esters and carboxylic acid; meanwhile, the adsorption band at 1237.918 cm^{-1} corresponds to an ether stretch (C-O-C). The vibration band around 999.966 cm^{-1} represents the C-C bonds in the fingerprint region. After activation and carbonization, there is the disappearance of some peaks in the FTIR spectra of the AgNP and a considerable decrease in the intensity of some peaks, as seen in Figure 3A. The peaks around 3297.338 and 1643.004 superimpose with those of AgNP. However, there is an outstanding similarity in the spectra of both AC and CNS. The band at 3264.76 cm^{-1} is attributed to the O-H bond stretching vibration of absorbed water molecules. The vibration band at 1643.004 cm^{-1} is attributed to the carbonyl group (C=O) of esters and carboxylic acid.

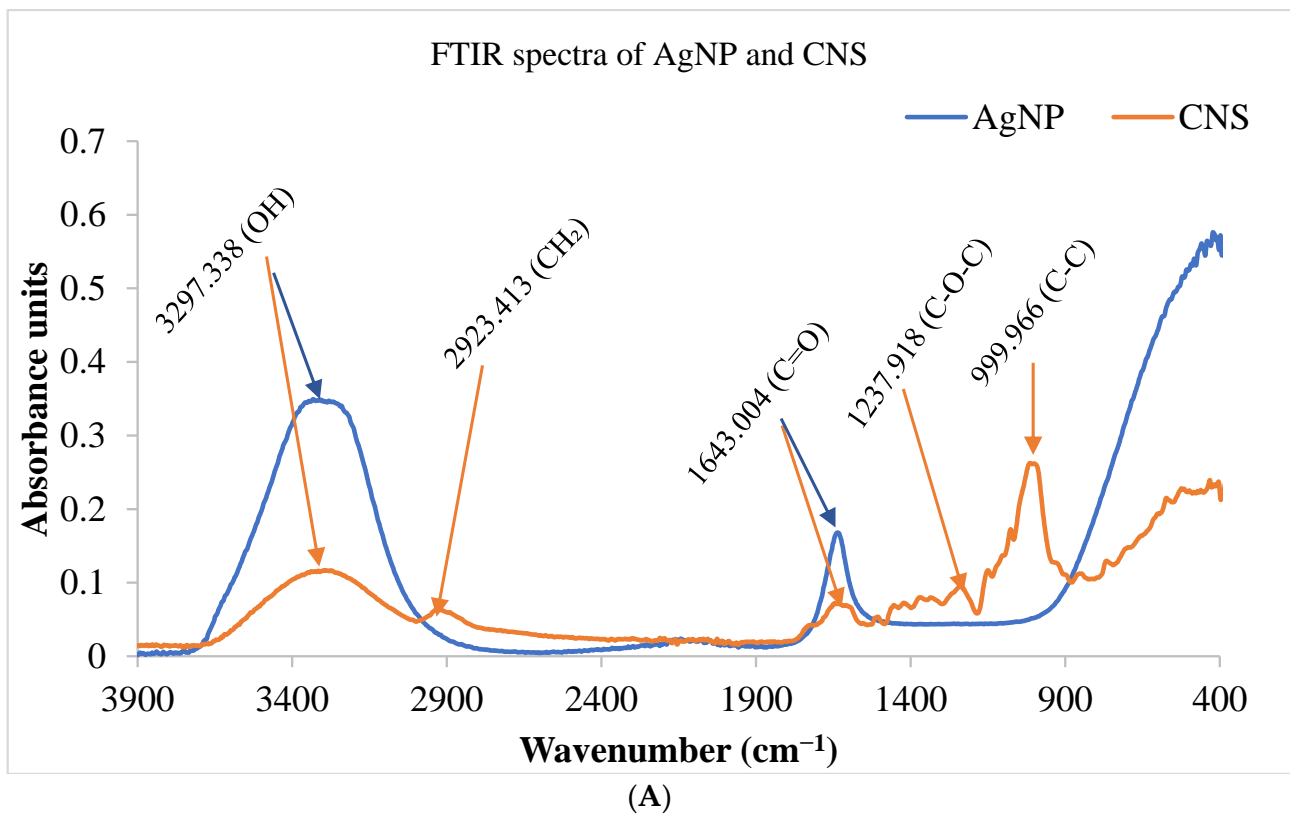


Figure 3. Cont.

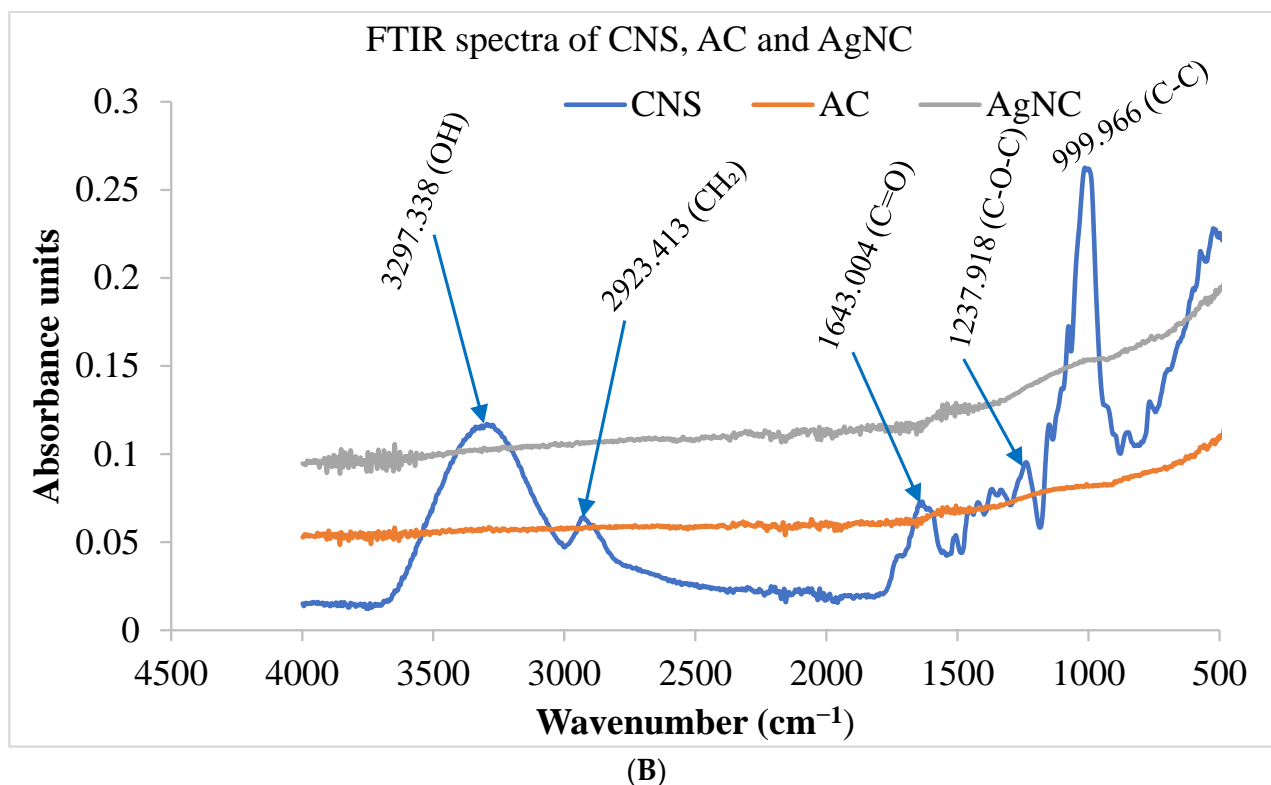


Figure 3. FTIR spectra of nanoparticles and coconut shell (A) coconut shell, activated carbon, and nanocomposites (B) prepared from *Cocos nucifera* aqueous extract. AC: activated carbon; CNS: *Cocos nucifera* extract; AgNC: silver nanocomposites; AgNPs: silver nanoparticles; FTIR: Fourier Transform Infrared Spectroscopy.

3.1.3. Minimum Inhibitory Concentrations of the As-Prepared Nanomaterials

a. MIC Values of Nanomaterials on Selected Bacteria

The incubation of different bacterial strains with various concentrations of nanoparticles (AgNP) led to a significant inhibition of the bacterial growth, as evidenced by the low MIC values obtained (Table 1). In fact, the MIC values ranged from 15.625 to 62.5 $\mu\text{g}/\text{mL}$, 15.625 to 31.25 $\mu\text{g}/\text{mL}$, and 7.8125 to 31.25 $\mu\text{g}/\text{mL}$ at 5, 10, and 20 mM, respectively. Similarly, the nanocomposite (AgNC) exhibited a significant antibacterial activity against the tested bacteria with MIC values ranging from 62.5 to 250 $\mu\text{g}/\text{mL}$, 31.25 to 250 $\mu\text{g}/\text{mL}$, and 31.25 to 62.5 $\mu\text{g}/\text{mL}$ at 5, 10, and 20 mM, respectively, vs. ciprofloxacin (MIC range: 0.039–0.156 $\mu\text{g}/\text{mL}$) (Table 1). Among the bacterial strains tested, *E. coli* was the most susceptible strain (for both nanomaterials), whereas *Salmonella enteritidis* (for the nanoparticle) and methicillin-resistant *Staphylococcus aureus*, *Klebsiella pneumoniae*, and *Shigella sonnei* (for the nanocomposite) were the most resistant bacterial strains.

b. MIC values of nanomaterials on selected fungi

Table 2 summarizes the minimum inhibitory concentrations (MICs) of the nanomaterials against selected fungi. The incubation of fungal strains with various concentrations of nanocomposites for 48 h resulted in the inhibition of fungal growth with minimum inhibitory concentrations (MICs) ranging from 31.25 to 125 $\mu\text{g}/\text{mL}$, 62.5 to 250 $\mu\text{g}/\text{mL}$, and 31.25 to 62.5 $\mu\text{g}/\text{mL}$ at the concentrations of 5, 10, and 20 mM, respectively, vs. fluconazole (MIC range: 0.153–0.3825 $\mu\text{g}/\text{mL}$). Likewise, the treatment of fungal strains with various concentrations of nanoparticles (5, 10, and 20 mM) resulted in the inhibition of tested fungi with minimum inhibitory concentrations ranging from 62.5 to 250 $\mu\text{g}/\text{mL}$, 62.5 to 250 $\mu\text{g}/\text{mL}$, and 31.25 to 62.5 $\mu\text{g}/\text{mL}$ at 5, 10, and 20 mM, respectively, vs. fluconazole (MIC range: 0.153–0.3825 $\mu\text{g}/\text{mL}$). Among the fungi tested, the most susceptible was found to be *Candida albicans* (MIC range: 7.812–31.25 $\mu\text{g}/\text{mL}$).

Table 1. Minimum inhibitory concentrations of the nanomaterials on selected bacterial strains.

Bacteria	Minimum Inhibitory Concentrations ($\mu\text{g/mL}$) ^a							
	EC	SONR	SA	SFNR	SAMR	SE	PANR	KPNR
AgNC 5 mM	62.5	125	62.5	250	250	250	125	62.5
AgNC 10 mM	31.25	250	62.5	62.5	125	125	62.5	62.5
AgNC 20 mM	31.25	62.5	31.25	31.25	62.5	31.25	31.25	62.5
AgNP 5 mM	15.625	62.5	15.625	31.25	31.25	31.25	31.25	31.25
AgNP 10 mM	15.625	62.5	15.625	31.25	15.625	125	15.625	31.25
AgNP 20 mM	7.8125	15.625	15.625	31.25	31.25	62.5	31.25	31.25
Ciprofloxacin	0.078	0.078	0.039	0.078	0.078	0.156	0.078	0.039

^a: Values are means of triplicate determination (n = 3); EC: *Escherichia coli*; KPNR: *Klebsiella pneumoniae*; SAMR: methicillin-resistant *Staphylococcus aureus*; PANR: *Pseudomonas aeruginosa*; SE: *Salmonella enteritidis*; SFNR: *Shigella flexneri*; SONR: *Shigella sonnei*; SA: *Staphylococcus aureus*; AgNC 5 mM: 5 mM silver nanocomposite; AgNC 10 mM: 10 mM silver nanocomposite; AgNC 20 mM: 20 mM silver nanocomposite; AgNP 5 mM: 5 mM silver nanoparticle; AgNP 10 mM: 10 mM silver nanoparticle; AgNP 20 mM: 20 mM silver nanoparticle.

Table 2. Minimum inhibitory concentrations of the nanomaterials on selected fungal strains.

Fungi	Minimum Inhibitory Concentrations ($\mu\text{g/mL}$) ^a				
	CK	CP	CG	CANR	CA
AgNC 5 mM	125	62.5	250	62.5	250
AgNC 10 mM	250	62.5	125	62.5	125
AgNC 20 mM	31.25	62.5	62.5	31.25	31.25
AgNP 5 mM	125	125	125	125	31.25
AgNP 10 mM	62.5	125	62.5	62.5	15.625
AgNP 20 mM	31.250	62.5	7.812	7.812	15.625
Fluconazole	0.153	0.153	0.3825	0.153	0.765

^a: Values are means of triplicate determination (n = 3); CA: *Candida albicans*, CANR: *Candida albicans*, CG: *Candida glabrata*, CK: *Candida krusei*, CP: *Candida parapsilosis*. AgNC 5 mM: 5 mM silver nanocomposite; AgNC 10 mM: 10 mM silver nanocomposite; AgNC 20 mM: 20 mM silver nanocomposite; AgNP 5 mM: 5 mM silver nanoparticle; AgNP 10 mM: 10 mM silver nanoparticle; AgNP 20 mM: 20 mM silver nanoparticle.

3.1.4. Time–Kill Kinetics

a. Time–kill kinetics in *Escherichia coli*

Since *E. coli* was found to be the most susceptible bacteria, the inhibitory potential of the nanomaterials was followed up at different time intervals for a period of 30 h at MIC/2, MIC and 2MIC. As a result, 8 to 10 hours of incubation of *E. coli*, along with MIC-based concentrations of nanomaterials (nanoparticle and nanocomposite), showed significant bacterial growth inhibition, as evidenced by a marked decrease in the bacterial growth curves of test samples compared with the negative control without treatment (Figure 4A,B) from 10 to 30 h of incubation time. The bacterial population significantly decreased, as shown by the curves' inclination towards the X axis. A similar trend was better observed with the standard drug ciprofloxacin (Figure 4A,B). These results demonstrate the bactericidal orientation of the nanomaterials at MIC and 2MIC.

b. Time–kill kinetics in *Candida albicans*

Since *Candida albicans* was found to be the most susceptible fungus, the inhibitory potential of the nanomaterials was followed up at different time intervals for a period of 48 h at MIC/2, MIC, and 2MIC. As a result, 8 to 10 hours of incubation of *C. albicans*, along with MIC-based concentrations of nanomaterials (nanoparticle and nanocomposite), showed significant inhibition of fungal growth, as evidenced by a marked decrease in the fungal growth curves of test samples compared with the negative control without treatment (Figure 5A,B). From 10 to 48 h of incubation time, there was a slight growth in the fungal population, as shown by the curves' inclination, which tends to be horizontal within the time period considered. A similar trend was observed with the standard drug fluconazole (Figure 5A,B). These results demonstrate the fungistatic inclination of the nanomaterials at MIC and 2MIC.

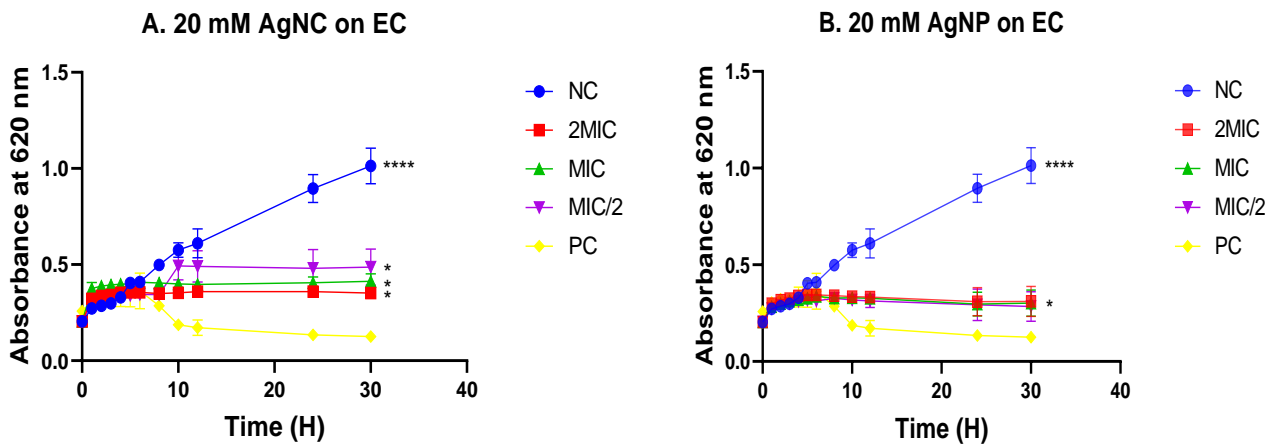


Figure 4. Time-kill curves of various concentrations of silver nanocomposite (A) and nanoparticle (B) on *Escherichia coli*. Data are presented as the mean \pm standard deviation. The graphs (curves) assigned to the stars are significantly different, (*) corresponds to $p < 0.05$, (****) corresponds to $p < 0.0001$ (Dunnett test); AgNC: 20 mM of silver nanocomposite; AgNP: 20 mM of silver nanoparticle; EC: *Escherichia coli*; NC: Negative control; PC: Positive control.

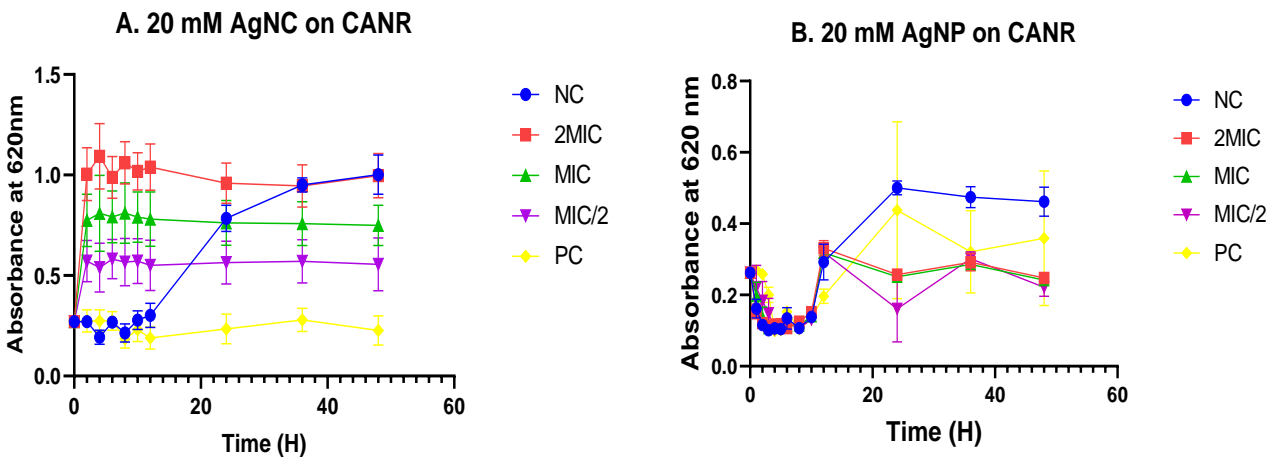


Figure 5. Time-kill curves of various concentrations of silver nanocomposite (A) and nanoparticle (B) on *Candida albicans*. Data are presented as the mean \pm standard deviation. The graphs (curves) are not significantly different ($p > 0.05$, Dunnett test); AgNC: 20 mM of silver nanocomposite; AgNP: 20 mM of silver nanoparticle; CANR: *Candida albicans*; NC: Negative control; PC: Positive control.

3.1.5. Cytotoxicity Assay

The cytotoxicity of the nanomaterials (nanoparticle and nanocomposite) was assayed on the human mammalian cells Vero. As a result, the incubation of nanocomposites with Vero cells did not affect the viability of the mammalian cells, as the median cytotoxic concentrations (CC_{50}) were calculated as $>1000 \mu\text{g/mL}$ at all the concentrations (5, 10, and 20 mM) tested. On the other hand, the incubation of the nanoparticle (AgNP) at 5 and 10 mM with the Vero cells did not cause any toxic effect on the cells because the CC_{50} values obtained were $>1000 \mu\text{g/mL}$; however, a 20 mM concentration of the AgNP revealed mild cytotoxicity toward Vero cells, as the CC_{50} value obtained was as low as $60.52 \mu\text{g/mL}$. Meanwhile, podophyllotoxin, the standard cytotoxic agent, yielded a CC_{50} value of $0.4 \mu\text{g/mL}$ (Table 3).

Table 3. Median cytotoxic concentrations.

Nanomaterials	CC ₅₀ (µg/mL) ^a
AgNC 5 mM	>1000
AgNC 10 mM	>1000
AgNC 20 mM	>1000
AgNP 5 mM	>1000
AgNP 10 mM	>1000
AgNP 20 mM	60.52 ± 0.070711
Podophyllotoxin	0.4 ± 0.1

^a: Values are means of triplicate determination (n = 3); AgNC 5 mM: 5 mM of silver nanocomposite; AgNC 10 mM: 10 mM of silver nanocomposite; AgNC 20 mM: 20 mM of silver nanocomposite; AgNP 5 mM: 5 mM of silver nanoparticle; AgNP 10 mM: 10 mM of silver nanoparticle; AgNP 20 mM: 20 mM of silver nanoparticle.

3.1.6. Antioxidant Activity

a. The DPPH scavenging assay

The DPPH assay revealed that 5 mM nanoparticle exhibited free radical scavenging activity with an RS₅₀ value of 382.5 ± 3.323 µg/mL, vs. ascorbic acid (RS₅₀ value: 7.363 µg/mL) (Table 4). Similar trends were observed for the median effective concentration (EC₅₀) (5 mM nanoparticle: 754.038 mol/µg, vs. ascorbic acid, 21.556 µg/mol) and antiradical potential (ARP) (5 mM nanoparticle: 198.529 mol/µg, vs. ascorbic acid, 104.46 mol/µg) (Table 4).

Table 4. DPPH radical scavenging activities of the nanomaterials.

Nanomaterials/ Ascorbic Acid	RSA ₅₀ (µg/mL)	EC ₅₀ × 10 ³ (µg/mol)	ARP × 10 ⁻⁶ (mol/µg)
AgNC 5 mM	>500	na	na
AgNC 10 mM	>500	na	na
AgNC 20 mM	>500	na	na
AgNP 5 mM	382.5 ± 3.323 ^b	754.038 ± 6.552 ^b	198.529 ± 0.0115 ^b
AgNP 10 mM	>500	na	na
AgNP 20 mM	>500	na	na
Ascorbic acid	7.363 ± 0.312 ^a	21.556 ± 0.615 ^a	104.46 ± 2.92 ^a

Data are represented as mean ± standard deviation. The values with different superscript letters (^a) and (^b) in a column are significantly different ($p < 0.05$), whereas the values carrying the same letter superscripts (^a) or (^b) are not significantly different ($p > 0.05$) (Dunnett's multiple comparisons test). AgNC 5 mM: 5 mM silver nanocomposite; AgNC 10 mM: 10 mM of silver nanocomposite; AgNC 20 mM: 20 mM of silver nanocomposite; AgNP 5 mM: 5 mM of silver nanoparticle; AgNP 10 mM: 10 mM of silver nanoparticle; AgNP 20 mM: 20 mM of silver nanoparticle, na: no activity.

b. The ABTS scavenging test

In the ABTS assay, the nanocomposite showed significant antioxidant activity at all the concentrations tested (5, 10, and 20 mM) (Table 5). At 10 and 20 mM, the nanocomposite exhibited better radical scavenging activities (RS₅₀ values: 8.2695 and 6.586 µg/mL) than ascorbic acid (RS₅₀ value: 22.46 µg/mL). In addition, the 5 mM nanocomposite presented significant antioxidant activity (RS₅₀ value: 53.855 µg/mL), even though the degree of the activity was less than that of ascorbic acid (RS₅₀ value: 22.46 µg/mL). The nanoparticle did not reveal significant ABTS scavenging activity at all the concentrations tested (RS₅₀: >500 µg/mL). In addition, the median effective concentrations (EC₅₀s) were found to be 15.387, 2.362, and 1.883 µg/mol at 5, 10, and 20 mM of nanocomposite, respectively. Moreover, the antioxidant radical potentials (ARP) were obtained as 6.619, 41.704, and 55.055 mol/µg at 5, 10, and 20 mM of nanocomposite, respectively, vs. ascorbic acid (ARP: 15.699 mol/µg) (Table 5).

Table 5. ABTS radical scavenging activities of the nanomaterials.

Nanomaterials/ Ascorbic Acid	RSA ₅₀ (µg/mL)	EC ₅₀ × 10 ³ (µg/mol)	ARP × 10 ⁻⁵ (mol/µg)
AgNC 5 mM	53.855 ± 2.722 ^a	15.387 ± 0.778 ^a	6.619 ± 1.703 ^a
AgNC 10 mM	8.2695 ± 0.353 ^a	2.362 ± 0.101 ^a	41.704 ± 8.765 ^a
AgNC 20 mM	6.586 ± 0.645 ^a	1.883 ± 0.186 ^a	55.055 ± 0.281 ^a
AgNP 5 mM	>500	na	na
AgNP 10 mM	>500	na	na
AgNP 20 mM	>500	na	na
Ascorbic acid	22.46 ± 2.729 ^a	6.417 ± 0.779 ^a	15.699 ± 0.19 ^a

Data are represented as mean ± standard deviation. The values with the same letter superscript (^a) are not significantly different ($p > 0.05$) (Dunnnett's multiple comparisons test). AgNC 5 mM: 5 mM silver of nanocomposite; AgNC 10 mM: 10 mM of silver nanocomposite; AgNC 20 mM: 20 mM of silver nanocomposite; AgNP 5 mM: 5 mM of silver nanoparticle; AgNP 10 mM: 10 mM of silver nanoparticle; AgNP 20 mM: 20 mM of silver nanoparticle, na: no activity.

3.2. Discussion

In this study, the aqueous extract of *Cocos nucifera* was used as a reducing and stabilizing agent for the bio-fabrication of silver nanoparticles. After preparing an activated carbon from this plant species, the as-prepared nanoparticles were loaded on activated carbon by simple impregnation to afford the nanocomposite. As it is essential that these materials be thoroughly characterized to ensure reproducibility in their fabrication, UV-vis spectrometry and FTIR analyses were used for the characterization of the as-prepared nanomaterials. As a result, the nanoparticles presented a λ_{max} value at 432 nm, which confirmed the synthesis of the nanoparticles, as it is well known that silver nanoparticles are formed at λ_{max} values within the visible range of 400–500 nm [47–49]. This result is consistent with a study by Das et al. [42], who recently prepared coconut-shell-based silver nanoparticles that displayed a maximum absorbance at 447 nm. The color change from colorless to dark brown was due to the presence of Ag nano-dot-embedded organic light-emitting diode by localized Surface Plasmon Resonance [50,51]. The intensity of the peaks shows the crystalline nature of the nanoparticles. A number of authors [52,53] have identified several phenolic compounds in *Cocos nucifera* shells, which might have contributed to the reduction in and stabilization of prepared nanoparticles. The FTIR analysis of *Cocos nucifera* aqueous extract, activated carbon, and the nanomaterials revealed a number of functional groups present at the surface of these materials. For instance, the main surface functional groups present in *C. nucifera* aqueous extract were a combination of hydroxyl (OH), methylene, carbonyl (C=O), and ether (C-O-C) groups, as evidenced by the report of Sulaeman and coworkers in 2016 [54]. As the *C. nucifera* aqueous extract is converted into silver nanoparticles using silver nitrate, there is a gradual change in the composition of the functional groups. For instance, there was a marked shift of peaks in the chromatogram of synthesized silver nanoparticles [26,55,56]. After activation and carbonization, all the functional groups present in the *C. nucifera* precursor disappeared due to the decomposition of cellulose, hemicellulose, and lignin during the carbonization process [57]. The disappearance of functional groups from the CNS to the activated carbon (AC) shows the effect of temperature and activating agents during the preparation of the AC. Nanoparticles and nanocomposites were further evaluated for antimicrobial activity against selected bacterial and fungal strains. As a result, these nanomaterials inhibited the growth of bacteria and fungi with MIC values ranging from 7.813 to 500 µg/mL. The most susceptible microorganisms were found to be *Escherichia coli* and *Candida albicans* among bacteria and fungi, respectively. It is worth noting that *Cocos nucifera* aqueous extract and activated carbon did not reveal antimicrobial activity (MIC > 1000 µg/mL); however, the role of these entities in the fabrication of nanomaterials with reduced toxicity and the enhancement of the antimicrobial activity is undeniable [42,56]. Through their small diameter, activated carbons efficiently bind onto microbes by adsorption to yield better or enhanced bactericidal properties [58,59]. Other features of activated carbons include high

porosity, high specific surface area, and desired surface functionalization [56,60]. Although there are almost no standard reported threshold values for antimicrobial nanomaterials to ascertain their degree of activity, it is generally known that the lower the MIC values of the test samples, the greater the antimicrobial activity. Other authors have speculated that very active and active antimicrobial plant extracts should exhibit MIC values $< 100 \mu\text{g/mL}$ and $100 \leq \text{MIC} \leq 512 \mu\text{g/mL}$, respectively [61,62]. Cytotoxic studies of 5 and 10 mM of the nanomaterials on the human mammalian cells Vero revealed no toxic effect, as evidenced by the median cytotoxic concentration (CC_{50} : $>1000 \mu\text{g/mL}$). At 20 mM concentration, the nanocomposite was not found to be toxic to Vero cells, whereas the nanoparticle showed mild cytotoxicity (CC_{50} : $60.52 \mu\text{g/mL}$) at this concentration. This observation might justify the plausible toxicity of nanoparticles over their nanocomposite counterparts. These results demonstrate that the antibacterial (SI: >16 to >32 and >16 to >128 for nanoparticle and nanocomposite, respectively) and antifungal (SI: >4 to >16 and >16 to >32 , for nanoparticle and nanocomposite, respectively) nanomaterials revealed high selectivity indices, thus highlighting the nontoxicity of these entities.

The kinetic of bacterial deaths, which was further evaluated, revealed a bactericidal orientation of the nanomaterials at MIC and 2MIC on *E. coli*, as evidenced by the trend of the curves obtained while plotting optical densities versus time of incubation. This observation helps conclude the existence of a putative mode by which *Cocos nucifera*-based nanomaterials affected bacterial growth. Indeed, there was a direct killing of bacteria for the overall period of incubation (30 h) studied, rather than an ephemeral inhibition of bacterial growth. It is worth noting that a decrease in the absorbance indicates a reduction in the bacterial population that might have resulted in the death of cells [63]. On the other hand, since *Candida albicans* was found to be the most susceptible fungus strain, the inhibitory potential of the nanomaterials was followed up at different time intervals for a period of 48 h at MIC/2, MIC, and 2MIC. As a result, 8 to 10 hours of incubation of *C. albicans*, along with MIC-based concentrations of nanomaterials, showed significant fungal growth inhibition, as evidenced by a marked decrease in the curves of test samples compared with the negative control without treatment (Figure 5A,B). From 10 to 48 h of incubation time, there was a slight growth in the fungal population, as shown by the curves' inclination, which tends to be horizontal within the entire time period considered. A similar trend was observed with the standard drug fluconazole (Figure 5A,B). These results demonstrate the fungistatic orientation of the nanomaterials at MIC and 2MIC.

Furthermore, the antimicrobial activity of nanoparticles has been attributed to three main mechanisms of action, including (i) adhesion onto the outer membrane, accumulation in the inner membrane, increase in membrane permeability, leakage of cell content followed by cell death; (ii) interaction with sulfur and phosphate groups of the DNA (deoxyribonucleic acid) and proteins to alter their functions; and (iii) interaction with cellular components to alter the metabolic pathways, membranes, and genetic material, among others [39,40,64,65].

As oxidative stress is intricately involved in any pathological condition, including infectious disease conditions, the antioxidant activity of the nanomaterials was evaluated to further detail whether the potential antioxidant activity of the nanomaterials might have contributed to their antibacterial action. In the DPPH assay, 5 mM of the nanoparticle showed antiradical activity, whereas in the ABTS test, the nanocomposite showed scavenging activity at all the concentrations tested (5, 10, and 20 mM). Several authors attributed the antioxidant activity of plant extracts or nanomaterials thereof to their abundance in a variety of polyphenols that are endowed with a high reducing capacity [66–68]. Both the nanomaterials revealed antioxidant activity, attesting to their implication in a plausible reduction of oxidative stress following microbial infection. Accumulating evidence has shown the involvement of oxidative stress in the pathogenesis of several diseases [69,70]; thus, the intervention of antioxidants during an infectious condition might prevent cell damage induced by oxidative stress.

Overall, *Cocos nucifera*-based nanomaterials were fabricated using an eco-friendly method. UV-vis and FTIR analyses were used to characterize these nanomaterials, which further exhibited concentration-dependent antibacterial and antifungal activities with no cytotoxic effects toward the human mammalian cells Vero. The mechanistic basis of the antibacterial action revealed a bactericidal orientation of the nanomaterials on *Escherichia coli* at MIC and 2MIC, whereas the antifungal action displayed a fungistatic inclination on *Candida albicans* at these concentrations, possibly through inhibition of the free radicals produced by the bacteria or fungi. This novel contribution has demonstrated the involvement of *Cocos nucifera*-based nanomaterials in targeting bacterial or fungal systems that mediate free radical damage or by inhibiting the oxidative impairment caused by selected bacteria and fungi.

4. Limitations and Perspectives

The present study describes the antimicrobial action of nanoscale materials from *Cocos nucifera* aqueous extract. *Cocos nucifera*-based nanoparticles and nanocomposites exhibited antibacterial and antifungal activities against a panel of selected bacteria and fungi, the most susceptible being *Escherichia coli* and *Candida albicans*, respectively. In addition, the mechanistic basis of the antibacterial action demonstrated that the nanomaterials induced (i) bactericidal orientation vis-à-vis *E. coli* at MIC and 2MIC, (iii) fungistatic inclination against *Candida albicans* at MIC and 2MIC, and (ii) free radical scavenging activity upon DPPH and ABTS assays. This novel contribution to the antimicrobial activity and potential mechanistic studies of *C. nucifera*-based nanoparticles and nanocomposite counterparts might allow a better understanding of the antimicrobial activity of these biomaterials. As it is essential that nanoscale materials be thoroughly characterized to ensure reproducibility in their fabrication, UV-vis spectrometry and FTIR analyses were used for the characterization of the as-prepared nanomaterials. However, major limitations of this study include the use of the latest generation of characterization techniques, such as TEM and XRD, among others, as a complement to provide a complete characterization of these nanomaterials. Nonetheless, to release a comprehensive characterization of the as-prepared nanomaterials, the assessment of morphological features, such as surface charge, crystal structure, and others, using TEM and XRD analyses should be considered among the main perspectives of this work. Furthermore, pharmacokinetic and in vivo studies, as well as in-depth antimicrobial mechanisms of action, should be investigated to warrant the successful utilization of these antimicrobial nanoscale materials.

5. Conclusions

This study reports the implication of *Cocos nucifera*-based nanomaterials in targeting bacterial or fungal systems by inhibiting the oxidative stress caused by selected bacteria and fungi. Thus, an eco-friendly method was used for the fabrication of nanoparticles using *Cocos nucifera* aqueous extract as the capping and reducing agent. The as-prepared nanoparticles were further impregnated with activated carbon (prepared from *Cocos nucifera*) to afford the nanocomposite. To our knowledge, this is the first report on the biological synthesis of nanocomposites from *Cocos nucifera* aqueous extract-based nanoparticles and activated carbon. Moreover, the nanomaterials were characterized using UV-vis spectroscopy and Fourier Transform Infrared (FTIR) spectroscopy. Upon in vitro antimicrobial assays of the nanomaterials against a panel of selected bacterial and fungal strains, there was a significant decrease in the bacterial and fungal loads, as evidenced by the low MIC range obtained for the nanoparticles (MIC range: 7.8125–250 µg/mL; SI range: >4 to >32; Vero cells) and the nanocomposite counterparts (MIC range: 31.25–250 µg/mL; SI range: >16 to >128; Vero cells). The time-kill kinetic studies of the antibacterial action against *E. coli* revealed bactericidal orientation at MIC and 2MIC, whereas antifungal action of the nanomaterials displayed a fungistatic trend vis-à-vis *Candida albicans* at these concentrations. The as-prepared nanomaterials exhibited antioxidant activity by scavenging free radicals of DPPH and ABTS. This novel research contribution has demonstrated the implication of

Cocos nucifera-based nanomaterials in targeting bacterial or fungal systems that mediate free radical damage or by inhibiting the oxidative impairment caused by selected bacteria and fungi, the most susceptible being *Escherichia coli* and *Candida albicans*, respectively.

Author Contributions: Conceptualization, P.K.L., J.N.N. and F.F.B.; methodology, Z.Y.T., N.O.A., A.L.M., F.L.T.T. and B.-N.N.-D.; software, V.N., B.-N.N.-D. and F.L.T.T.; validation, P.K.L., J.N.N. and F.F.B.; formal analysis, Z.Y.T., F.L.T.T., N.O.A., A.L.M., B.P.K. and V.N.; investigation, Z.Y.T., F.L.T.T., N.O.A., A.L.M., B.-N.N.-D., B.P.K. and V.N.; resources, P.K.L., J.N.N., B.P.K. and F.F.B.; data curation, Z.Y.T., F.L.T.T., N.O.A., A.L.M., B.-N.N.-D. and V.N.; writing—original draft preparation, Z.Y.T., F.L.T.T. and V.N.; writing—review and editing, Z.Y.T. and B.P.K.; visualization, P.K.L., B.P.K. and J.N.N.; supervision, P.K.L., J.N.N. and F.F.B.; project administration, P.K.L., J.N.N., B.P.K. and F.F.B.; funding acquisition, P.K.L., B.P.K., J.N.N. and F.F.B. All authors have read and agreed to the published version of the manuscript.

Funding: This work was externally funded by the Yaounde-Bielefeld Bilateral Graduate School for Natural Products with Anti-parasite and Antibacterial Activity (YaBiNaPA) (grant number 57316173) and the Seeding Labs' Instrumental Access.

Institutional Review Board Statement: Not applicable.

Informed Consent Statement: Not applicable.

Data Availability Statement: Data are available from the corresponding author upon reasonable request.

Acknowledgments: The authors would like to thank the “Centre Hospitalier Universitaire” of Yaounde (Cameroon) and “Centre Pasteur” of Cameroon for providing the bacterial and fungal strains. This work received support from the Yaoundé-Bielefeld Bilateral Graduate School for Natural Products with Anti-parasite and Antibacterial Activity (YaBiNaPA) and the Seeding Labs' Instrumental Access.

Conflicts of Interest: The authors declare no conflicts of interest.

References

1. The World Health Organization (WHO). Infectious Diseases. The Fact Sheets 2024. Available online: <https://www.emro.who.int/health-topics/infectious-diseases/index.html> (accessed on 6 January 2024).
2. Nii-Trebi, N.I. Emerging and neglected infectious diseases: Insights, advances, and challenges. *Biomed. Res. Int.* **2017**, *2017*, 5245021. [CrossRef]
3. Kumwenda, P.; Adukwu, E.C.; Tabe, E.S.; Ujor, V.C.; Kamudumuli, P.S.; Ngwira, M.; Tsung, J.; Wu, S.; Chisale, M.R.O. Prevalence, distribution and antimicrobial susceptibility pattern of bacterial isolates from a tertiary Hospital in Malawi. *BMC Infect. Dis.* **2021**, *21*, 34. [CrossRef]
4. Bongomin, F.; Gago, S.; Oladele, R.O.; Denning, D.W. Global and multi-national prevalence of fungal diseases-estimate precision. *J. Fungi* **2017**, *3*, 57. [CrossRef]
5. Kainz, K.; Bauer, M.A.; Madeo, F.; Carmona-gutierrez, D. Fungal infections in humans: The silent crisis. *Microb. Cell* **2022**, *7*, 143–145. [CrossRef]
6. Pfavayi, L.T.; Denning, D.W.; Baker, S.; Sibanda, E.N.; Mutapi, F. Determining the burden of fungal infections in Zimbabwe. *Sci. Rep.* **2021**, *11*, 13240. [CrossRef] [PubMed]
7. Mandengue, C.E.; Denning, D.W. The burden of serious fungal infections in Cameroon. *J. Fungi* **2018**, *4*, 44. [CrossRef] [PubMed]
8. Dall, C. Report Highlights the Deadly Impact of Bacterial Infections. Antimicrobial Stewardship Public Health. CIDRAP. 2022. Available online: <https://www.cidrap.umn.edu/antimicrobial-stewardship/report-highlights-deadly-impact-bacterial-infections> (accessed on 21 January 2024).
9. Muendlein, H. Bacterial Infections Caused Most Deaths in Sub-Saharan Africa in 2019. *Lancet* **2022**. Available online: <https://www.downtoearth.org.in/news/africa/bacterial-infections-caused-most-deaths-in-sub-saharan-africa-in-2019-lancet-86209#:~:text=Published:%20Monday%2028%20November%202022&text=Sub-Saharan%20Africa%20saw%20the,cause%20of%20death%20in%202019> (accessed on 22 January 2024).
10. AMvomo, N.L.D.; Sama, C.K.K.; Bouopda, R.; Minkeza, F.C.N.; Mbopda, L.P.; Tchoumi, C.L.Y.; Kenmoe, L.O.T.; Simeni, G.T.; Tolo, E.C.; Ngongang, R.; et al. Bacterial ecology and antibiotic susceptibility profile of isolated strains from surfaces and medical devices in some departments of the Jordan Medical Services, Cameroon: A descriptive cross-sectional study. *PAMJ One Health* **2023**, *11*, 6. [CrossRef]
11. Segal, E.; Elad, D. Special issue: Treatments for fungal infections. *J. Fungi* **2018**, *4*, 135. [CrossRef] [PubMed]

12. Leekha, S.; Terrell, C.L.; Edson, R.S. General principles of antimicrobial therapy. *Mayo Clin. Proc.* **2011**, *86*, 156–167. [[CrossRef](#)] [[PubMed](#)]
13. Giurazza, R.; Mazza, M.C.; Andini, R.; Sansone, P.; Pace, M.C.; Durante-Mangoni, E. Emerging treatment options for multi-drug-resistant bacterial infections. *Life* **2021**, *11*, 519. [[CrossRef](#)] [[PubMed](#)]
14. Campitelli, M.; Zeineddine, N.; Samaha, G.; Maslak, S. Combination antifungal therapy: A review of current data. *J. Clin. Med. Res.* **2017**, *9*, 451–456. [[CrossRef](#)] [[PubMed](#)]
15. Johnson, M.D.; MacDougall, C.; Ostrosky-Zeichner, L.; Perfect, J.R.; Rex, J.H. Combination antifungal therapy. *Antimicrob. Agents Chemother.* **2004**, *48*, 693–715. [[CrossRef](#)] [[PubMed](#)]
16. Wahab, M.A.; Li, L.; Li, H.; Abdala, A. Silver nanoparticle-based nanocomposites for combating infectious pathogens: Recent advances and future prospects. *Nanomaterials* **2021**, *11*, 581. [[CrossRef](#)]
17. Vaou, N.; Stavropoulou, E.; Voidarou, C.C.; Tsakris, Z.; Rozos, G.; Tsigalou, C.; Bezirtzoglou, E. Interactions between medical plant-derived bioactive compounds: Focus on antimicrobial combination effects. *Antibiotics* **2022**, *11*, 1014. [[CrossRef](#)]
18. Nguimatsia, F.; Kenmogne, S.B.; Ngo Mback, M.N.L.; Kouamouo, J.; Nzenti Tchuitio, L.L.; Melogmo Dongmo, Y.K.; Jazet Dongmo, P.M. Antibacterial activities of the essential oil and hydroethanolic extract from *Aeollanthus heliotropioides* Oliv. *Mediterr. J. Chem.* **2021**, *11*, 95–103.
19. Lima, E.B.; Sousa, C.N.; Meneses, L.N.; Ximenes, N.C.; Santos Júnior, M.A.; Vasconcelos, G.S.; Lima, N.B.; Patrocínio, M.C.; Macedo, D.; Vasconcelos, S.M. *Cocos nucifera* (L.) (Arecaceae): A phytochemical and pharmacological review. *Braz. J. Med. Biol. Res.* **2015**, *48*, 953–964. [[CrossRef](#)]
20. Jadimurthy, R.; Jagadish, S.; Nayak, S.C.; Kumar, S.; Mohan, C.D.; Rangappa, K.S. Phytochemicals as invaluable sources of potent antimicrobial agents to combat antibiotic resistance. *Life* **2023**, *13*, 948. [[CrossRef](#)]
21. Patra, J.K.; Das, G.; Fraceto, L.F.; Campos, E.V.R.; Rodriguez-Torres, M.d.P.; Acosta-Torres, L.S.; Diaz-Torres, L.A.; Grillo, R.; Swamy, M.K.; Sharma, S.; et al. Nano based drug delivery systems: Recent developments and future prospects. *J. Nanobiotechnol.* **2018**, *16*, 71. [[CrossRef](#)] [[PubMed](#)]
22. Yin, I.X.; Zhang, J.; Zhao, I.S.; Mei, M.L.; Li, Q.; Chu, C.H. The antibacterial mechanism of silver nanoparticles and its application in dentistry. *Int. J. Nanomed.* **2020**, *15*, 2555–2562. [[CrossRef](#)] [[PubMed](#)]
23. Bruna, T.; Maldonado-Bravo, F.; Jara, P.; Caro, N. Silver nanoparticles and their antibacterial applications. *Int. J. Mol. Sci.* **2021**, *22*, 7202. [[CrossRef](#)]
24. Gudkov, S.V.; Serov, D.A.; Astashev, M.E.; Semenova, A.A.; Lisitsyn, A.B. Ag₂O nanoparticles as a candidate for antimicrobial compounds of the new generation. *Pharmaceuticals* **2022**, *15*, 968. [[CrossRef](#)]
25. Sánchez-López, E.; Gomes, D.; Esteruelas, G.; Bonilla, L.; Lopez-Machado, A.L.; Galindo, R.; Cano, A.; Espina, M.; Ettcheto, M.; Camins, A.; et al. Metal-based nanoparticles as antimicrobial agents: An overview. *Nanomaterials* **2020**, *10*, 292. [[CrossRef](#)]
26. Taha, A.; Ben Aissa, M.; Da’na, E. Green synthesis of an activated carbon-supported Ag and ZnO nanocomposite for photocatalytic degradation and its antibacterial activities. *Molecules* **2020**, *25*, 1586. [[CrossRef](#)] [[PubMed](#)]
27. Franco, D.; Calabrese, G.; Guglielmino, S.P.P.; Conoci, S. Metal-based nanoparticles: Antibacterial mechanisms and biomedical application. *Microorganisms* **2022**, *10*, 1778. [[CrossRef](#)] [[PubMed](#)]
28. Javed, R.; Zia, M.; Naz, S.; Aisida, S.O.; Ain, N.-u.; Ao, Q. Role of capping agents in the application of nanoparticles in biomedicine and environmental remediation: Recent trends and future prospects. *J. Nanobiotechnol.* **2020**, *18*, 172. [[CrossRef](#)] [[PubMed](#)]
29. Xulu, J.H.; Ndongwe, T.; Ezealisiji, K.M.; Tembu, V.J.; Mncwangi, N.P.; Witika, B.A.; Siwe-Noundou, X. The use of medicinal plant-derived metallic nanoparticles in theranostics. *Pharmaceutics* **2022**, *14*, 2437. [[CrossRef](#)] [[PubMed](#)]
30. Ghazzy, A.; Naik, R.R.; Shakya, A.K. Metal-polymer nanocomposites: A promising approach to antibacterial materials. *Polymers* **2023**, *15*, 2167. [[CrossRef](#)] [[PubMed](#)]
31. Pongener, C.; Kibami, D.; Rao, K.S.; Goswamee, R.L.; Sinha, D. Adsorption studies of fluoride by activated carbon prepared from *Mucuna prurines* plant. *Biological Methods of Water Treatment. J. Water Chem. Technol.* **2017**, *39*, 108–115. [[CrossRef](#)]
32. Suriyaprom, S.; Mosoni, P.; Leroy, S.; Kaewkod, T.; Desvaux, M.; Tragoolpua, Y. Antioxidants of fruit extracts as antimicrobial agents against pathogenic bacteria. *Antioxidants* **2022**, *11*, 602. [[CrossRef](#)] [[PubMed](#)]
33. Parusnath, M.; Naidoo, Y.; Singh, M.; Kianersi, F.; Dewir, Y.H. Antioxidant and antibacterial activities of the leaf and stem extracts of *Combretum molle* (R. Br. ex G. Don.) Engl. & Diels. *Plants* **2023**, *12*, 1757. [[CrossRef](#)] [[PubMed](#)]
34. Gómez-Tah, R.; Islas-Flores, I.; Félix, J.W.; Granados-Alegría, M.I.; Tzec-Simá, M.; Guerrero-Analco, J.A.; Monribo-Villanueva, J.L.; Canto-Canché, B. Untargeted metabolomics analysis of liquid endosperm of *Cocos nucifera* L. at three stages of maturation evidenced differences in metabolic regulation. *Horticulturae* **2023**, *9*, 866. [[CrossRef](#)]
35. Beveridge, F.C.; Kalaipandian, S.; Yang, C.; Adkins, S.W. Fruit Biology of coconut (*Cocos nucifera* L.). *Plants* **2022**, *11*, 3293. [[CrossRef](#)] [[PubMed](#)]
36. Leliana, L.; Setyaningsih, W.; Palma, M.; Supriyadi; Santoso, U. Antioxidant activity of aqueous and ethanolic extracts of coconut (*Cocos nucifera*) fruit by-products. *Agronomy* **2022**, *12*, 1102. [[CrossRef](#)]
37. Mikłasińska-Majdanik, M.; Kepa, M.; Wojtyczka, R.D.; Idzik, D.; Wasik, T.J. Phenolic compounds diminish antibiotic resistance of *Staphylococcus aureus* clinical strains. *Int. J. Environ. Res. Public Health* **2018**, *15*, 2321. [[CrossRef](#)] [[PubMed](#)]
38. Shamsudin, N.F.; Ahmed, Q.U.; Mahmood, S.; Ali Shah, S.A.; Khatib, A.; Mukhtar, S.; Alsharif, M.A.; Parveen, H.; Zakaria, Z.A. Antibacterial effects of flavonoids and their structure-activity relationship study: A comparative interpretation. *Molecules* **2022**, *27*, 1149. [[CrossRef](#)] [[PubMed](#)]

39. Wiart, C.; Kathirvalu, G.; Raju, C.S.; Nissapatorn, V.; Rahmatullah, M.; Paul, A.K.; Rajagopal, M.; Sathiya Seelan, J.S.; Rusdi, N.A.; Lanting, S.; et al. Antibacterial and antifungal terpenes from the medicinal angiosperms of Asia and the Pacific: Haystacks and gold needles. *Molecules* **2023**, *28*, 3873. [[CrossRef](#)] [[PubMed](#)]
40. Silva, V.; Silva, A.; Ribeiro, J.; Aires, A.; Carvalho, R.; Amaral, J.S.; Barros, L.; Igrejas, G.; Poeta, P. Screening of chemical composition, antimicrobial and antioxidant activities in pomegranate, quince, and persimmon leaf, peel, and seed: Valorization of autumn fruits by-products for a one health perspective. *Antibiotics* **2023**, *12*, 1086. [[CrossRef](#)]
41. Naphtali Odogu, A.; Daouda, K.; Paul, L.K.; Agbor Tabi, G.; Ngouateu Rene, L.; Nsami, N.J.; Mbadcam, K.K. Effect of doping activated carbon based *Ricinodendron Heudelotti* shells with AgNPs on the adsorption of indigo carmine and its antibacterial properties. *Arab. J. Chem.* **2020**, *13*, 5241–5253. [[CrossRef](#)]
42. Das, G.; Shin, H.S.; Kumar, A.; Vishnuprasad, C.N.; Patra, J.K. Photo-mediated optimized synthesis of silver nanoparticles using the extracts of outer shell fibre of *Cocos nucifera* L. fruit and detection of its antioxidant, cytotoxicity and antibacterial potential. *Saudi J. Biol. Sci.* **2021**, *28*, 980–987. [[CrossRef](#)]
43. Clinical Laboratory Standards Institute (CLSI). *Methods for Dilution Antimicrobial Susceptibility Tests for Bacteria That Grow Aerobically*; Approved Standard-Ninth Edition M07 A9; Clinical Laboratory Standards Institute: Wayne, PA, USA, 2012; p. 29.
44. Bowling, T.; Mercer, L.; Don, R.; Jacobs, R.; Nare, B. Application of a resazurin-based high-throughput screening assay for the identification and progression of new treatments for human African trypanosomiasis. *Int. J. Parasitol. Drugs Drug Resist.* **2012**, *2*, 262–270. [[CrossRef](#)]
45. Bassene, E. *Initiation à la Recherche sur les Substances Naturelles*; Presse Universitaire de Dakar: Dakar, Senegal, 2012; 147p.
46. Khan, R.A.; Khan, M.R.; Sahreen, S.; Ahmed, M. Evaluation of phenolic contents and antioxidant activity of various solvent extracts of *Sonchus asper* (L.) Hill. *Chem. Cent. J.* **2012**, *6*, 12. [[CrossRef](#)]
47. Sinsinwar, S.; Sarkar, M.K.; Suriya, K.R.; Nithyanand, P.; Vadivel, V. Use of agricultural waste (coconut shell) for the synthesis of silver nanoparticles and evaluation of their antibacterial activity against selected human pathogens. *Microb. Pathog.* **2018**, *124*, 30–37. [[CrossRef](#)]
48. Alshehri, A.A.; Malik, M.A. Phytomediated photo-induced green synthesis of silver nanoparticles using *Matricaria chamomilla* L. and its catalytic activity against rhodamine B. *Biomolecules* **2020**, *10*, 1604. [[CrossRef](#)]
49. Hano, C.; Abbasi, B.H. Plant-based green synthesis of nanoparticles: Production, characterization and applications. *Biomolecules* **2021**, *12*, 31. [[CrossRef](#)]
50. Lee, I.; Park, J.Y.; Hong, K.; Son, J.H.; Kim, S.; Lee, J.L. The effect of localized surface Plasmon resonance on the emission colour change in organic light emitting diodes. *Nanoscale* **2016**, *8*, 6463–6467. [[CrossRef](#)]
51. Rautela, A.; Rani, J.; Debnath (Das), M. Green synthesis of silver nanoparticles from *Tectona grandis* seeds extract: Characterization and mechanism of antimicrobial action on different microorganisms. *J. Anal. Sci. Technol.* **2019**, *10*, 5. [[CrossRef](#)]
52. Paul, K.; Bag, B.G.; Samanta, K. Green coconut (*Cocos nucifera* Linn) shell extract mediated size controlled green synthesis of polyshaped gold nanoparticles and its application in catalysis. *Appl. Nanosci.* **2014**, *4*, 769–775. [[CrossRef](#)]
53. Khalid Thebo, N.; Ahmed Simair, A.; Sughra Mangrio, G.; Ansari, K.; Ali Bhutto, A.; Lu, C.; Ali Sheikh, W. Antifungal potential and antioxidant efficacy in the shell extract of *Cocos nucifera* (L.) (Arecaceae) against pathogenic dermal mycosis. *Medicines* **2016**, *3*, 12. [[CrossRef](#)]
54. Sulaeman, A.; Mathematics, F.; Sciences, N.; Bandung, I.T. Preliminary study of characterization of nanoparticles from coconut shell as filler agent in composites materials. *MAYFEB J. Mater. Sci.* **2016**, *1*, 1–9.
55. Kumari, B.V.; Mani, R.; Asokan, B.R.; Balakrishnan, K.; Ramasamy, A.; Parthasarathi, R.; Kandasamy, C.; Govindaraj, R.; Vijayakumar, N.; Vijayakumar, S. Green synthesised silver nanoparticles using *Anoectochilus elatus* leaf extract: Characterisation and evaluation of antioxidant, anti-inflammatory, antidiabetic, and antimicrobial activities. *J. Compos. Sci.* **2023**, *7*, 453. [[CrossRef](#)]
56. Franklin Loic, T.T.; Boniface, P.K.; Vincent, N.; Zuriatou, Y.T.; Yimgang, V.L.; Ndi, J.N.; Paul, K.L.; Fabrice, F.B. Biological synthesis and characterization of silver-doped nanocomposites: Antibacterial and mechanistic studies. *Drugs Drug Candidates* **2024**, *3*, 13–32.
57. Yahya, M.A.; Mansor, M.H.; Zolkarnaini, W.A.A.W.; Rusli, N.S.; Aminuddin, A.; Mohamad, K.; Sabhan, F.A.M.; Atik, A.A.A.; Ozair, L.N. A brief review on activated carbon derived from agriculture by-product. *AIP Conf. Proc.* **2018**, *1972*, 030023. [[CrossRef](#)]
58. Mikhailova, E.O. Silver Nanoparticles: Mechanism of action and probable bio-application. *J. Funct. Biomater.* **2020**, *11*, 84. [[CrossRef](#)]
59. Burchacka, E.; Pstrowska, K.; Bryk, M.; Maciejowski, F.; Kułazyński, M.; Chojnacka, K. The properties of activated carbons functionalized with an antibacterial agent and a new SufA protease inhibitor. *Materials* **2023**, *16*, 1263. [[CrossRef](#)]
60. Alvarez-Galvan, Y.; Minofar, B.; Futera, Z.; Francoeur, M.; Jean-Marius, C.; Brehm, N.; Yacou, C.; Jauregui-Haza, U.J.; Gaspard, S. Adsorption of hexavalent chromium using activated carbon produced from *Sargassum* ssp.: Comparison between lab experiments and molecular dynamics simulations. *Molecules* **2022**, *27*, 6040. [[CrossRef](#)]
61. Tamokou, J.d.D.; Mbaveng, A.T.; Kuete, V. Antimicrobial Activities of African Medicinal Spices and Vegetables. In *Medicinal Spices and Vegetables from Africa: Therapeutic Potential Against Metabolic, Inflammatory, Infectious and Systemic Diseases*; Elsevier: Amsterdam, The Netherlands, 2017; pp. 207–237.
62. Brice, R.P.; Boniface, P.K.; Eutrophe Le Doux, K.; Vincent, N.; Yanick Kevin, M.D.; Paul, K.L.; Fabrice, F.B. Extracts from *Cardiospermum grandiflorum* and *Blighia welwitschii* (Sapindaceae) reveal antibacterial activity against *Shigella* species. *S. Afr. J. Bot.* **2023**, *164*, 419–428.

63. Majoumouo, M.S.; Sibuyi, N.R.S.; Tincho, M.B.; Mbekou, M.; Boyom, F.F.; Meyer, M. Enhanced anti-bacterial activity of biogenic silver nanoparticles synthesized from *Terminalia mantaly* extracts. *Int. J. Nanomed.* **2019**, *14*, 9031–9046. [[CrossRef](#)]
64. Basavegowda, N.; Baek, K.-H. Combination strategies of different antimicrobials: An efficient and alternative tool for pathogen inactivation. *Biomedicines* **2022**, *10*, 2219. [[CrossRef](#)]
65. Lobiuc, A.; Pavăl, N.-E.; Mangalagiu, I.I.; Gheorghită, R.; Teliban, G.-C.; Amăriucăi-Mantu, D.; Stoleru, V. Future antimicrobials: Natural and functionalized phenolics. *Molecules* **2023**, *28*, 1114. [[CrossRef](#)]
66. Villaño, D.; Fernández-Pachón, M.; Moyá, M.; Troncoso, A.; García-Parrilla, M. Radical scavenging ability of polyphenolic compounds towards DPPH free radical. *Talanta* **2007**, *1*, 230–235. [[CrossRef](#)]
67. Flieger, J.; Franus, W.; Panek, R.; Szymańska-Chargot, M.; Flieger, W.; Flieger, M.; Kołodziej, P. Green synthesis of silver nanoparticles using natural extracts with proven antioxidant activity. *Molecules* **2021**, *26*, 4986. [[CrossRef](#)] [[PubMed](#)]
68. Ahmed, M.; Marrez, D.A.; Abdelmoeen, N.M.; Mahmoud, E.A.; Abdel-Shakur Ali, M.; Decsi, K.; Tóth, Z. Studying the antioxidant and the antimicrobial activities of leaf successive extracts compared to the green-chemically synthesized silver nanoparticles and the crude aqueous extract from *Azadirachta indica*. *Processes* **2023**, *11*, 1644. [[CrossRef](#)]
69. Ivanov, A.V.; Bartosch, B.; Isaguliant, M.G. Oxidative Stress in Infection and Consequent Disease. *Oxid. Med. Cell Longev.* **2017**, *2017*, 3496043. [[CrossRef](#)] [[PubMed](#)]
70. Cancemi, G.; Cicero, N.; Allegra, A.; Gangemi, S. Effect of diet and oxidative stress in the pathogenesis of lymphoproliferative disorders. *Antioxidants* **2023**, *12*, 1674. [[CrossRef](#)]

Disclaimer/Publisher’s Note: The statements, opinions and data contained in all publications are solely those of the individual author(s) and contributor(s) and not of MDPI and/or the editor(s). MDPI and/or the editor(s) disclaim responsibility for any injury to people or property resulting from any ideas, methods, instructions or products referred to in the content.